ACS APPLIED MATERIALS & INTERFACES

Research Article

Cite This: ACS Appl. Mater. Interfaces 2018, 10, 21965−21972

www.acsami.org

Minimizing Polysulfide Shuttle Effect in Lithium-Ion Sulfur Batteries by Anode Surface Passivation

Jian Liu,[†,∥] Dongping Lu,[*,†] Jianming Zheng,[†] Pengfei Yan,[‡] Biqiong Wang,[§] Xueliang Sun,[§] Yuyan Shao,[†] Chongmin Wang,[‡] Jie Xiao,[†] Ji-Guang Zhang,[†] and Jun Liu[*,†]

[†]Energy & Environment Directorate, Pacific Northwest National Laboratory, Richland, Washington 99354 United States

[‡]Environmental Molecular Sciences Laboratory, Pacific Northwest National Laboratory, Richland, Washington 99354 United States

[§]Department of Mechanical and Materials Engineering, University of Western Ontario, London, Ontario N6A 5B9 Canada

[∥]School of Engineering, Faculty of Applied Science, University of British Columbia, Kelowna, British Columbia V1 V 1 V7 Canada

Supporting Information

ABSTRACT: Lithium-ion sulfur batteries use nonlithium materials as the anode for extended cycle life. However, polysulfide shuttle reactions still occur on the nonmetal anodes (such as graphite and Si), and result in undesirable low Coulombic efficiency. In this work, we used Al_2O_3 layers coated by atomic layer deposition (ALD) technique to suppress the shuttle reactions. With the optimal thickness of 2 nm Al_2O_3 coated on graphite anode, the Coulombic efficiency of the sulfur cathode was improved from 84% to 96% in the first cycle, and from 94% to 97% in the subsequent cycles. As a result, the discharge capacity of the sulfur cathode was increased to 550 mAh g^{-1} in the 100th cycle, as compared with 440 mAh g^{-1} when the pristine graphite anode was used. The Al_2O_3 passivation layer minimizes the formation of insoluble sulfide (Li_2S_2, Li_2S) on the surface of graphite anode and improves the efficiency and capacity retention of the graphite-sulfur batteries. The surface passivation strategy could also be used in other sulfur based battery systems (with Li, Si, and Sn anodes), to minimize side reactions and enable high-performance sulfur batteries.

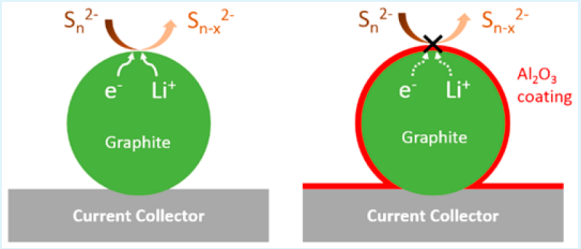

KEYWORDS: *lithium-ion sulfur battery, surface coating, atomic layer deposition, shuttle effect, graphite*

1. INTRODUCTION

Lithium−sulfur (Li−S) batteries have gained significant attention as a competitive power supply system for electric vehicles because of their high theoretical energy density (1675 mAh g^{-1}), natural abundance, and low cost of elemental sulfur.[1−4] Li−S batteries operate based on Li metal plating/stripping on the anode and sulfur conversion reactions on the cathode and exhibit a specific theoretical capacity five times greater than that of state-of-the-art Li-ion batteries.[5] Despite of these attractive advantages, the present Li−S batteries are still limited in the cycling life, efficiency, and energy density because of several formidable challenges, such as polysulfide shuttle effect, poor conductivity of sulfur and solid discharge products, and instability of Li metal.[5−7] During the past few years, encouraging progresses have been made to develop novel cathode structure to address the polysulfide shuttle effect and poor conductivity of sulfur.[1,2,8,9] However, the problems associated with Li metal remain unresolved. Li metal anode suffers from dendrite growth and serious polysulfide corrosion, which could accelerate the depletion of electrolytes and cause low Coulombic efficiency (CE) of Li−S batteries because of the absence of a stable solid electrolyte interphase (SEI).[10,11] These problems become even more detrimental in Li−S batteries in which thick sulfur cathodes (sulfur loading >3 mg cm^{-2}) are used.[5,12,13]

Several approaches have been developed to circumvent the problems in Li metal for sulfur batteries, such as electrolyte additives,[14] physical protection,[15] hybrid anode,[16] and solid-state electrolytes.[17] Another alternative route is to pair a non-Li anode (such as Si, hard carbon, and graphite), instead of Li metal, with the sulfur cathode to develop Li-ion sulfur batteries.[18−22] The advantages of non-Li anodes are that they are free of Li dendrite growth and show much less reactivity with liquid electrolytes than Li metal. For example, Cui and co-workers demonstrated the feasibility of replacing Li metal with Si nanowires. In combination with a Li_2S/mesoporous carbon cathode, the cell delivered a discharge capacity of 500 mAh g_{sulfur}^{-1} in the first cycle.[18] Aurbach showed a full silicon−sulfur battery prototype by using a prelithiated amorphous Si anode and a sulfur cathode. The reversible capacity was 600 mAh g_{sulfur}^{-1} at the first 10 cycles, and gradually faded to ∼380 mAh g_{sulfur}^{-1} after 60 cycles.[19] Besides alloy-type anodes, hard carbon has also been used as the anode with sulfur cathodes, and the full cell exhibited a capacity of 753 mAh g_{sulfur}^{-1} in the 550th cycle without cell failure.[20] Although graphite was reported to be unstable in ether-based electrolytes due to Li-ion

Received: February 8, 2018
Accepted: June 7, 2018
Published: June 7, 2018

DOI: 10.1021/acsami.8b02381
ACS Appl. Mater. Interfaces 2018, 10, 21965−21972

solvent cointercalation, recent work has demonstrated that it could be stabilized and used as the anode in sulfur batteries, by using a poly(acrylic acid) binder[21] or a concentrated electrolyte.[22] These works suggested that using non-Li anode is a promising approach to develop safe and practical sulfur batteries before successfully addressing all those issues associated with Li metal. Nevertheless, polysulfide shuttle reactions still occur when using non-Li anodes, leading to limited cycling life and low CE in Li-ion sulfur batteries.[18,19,22] For example, a thick SEI layer was found to form in the Si anode upon cycling, due to polysulfide shuttle reactions and large volume change of Si.[19] This thick SEI was believed to be responsible for the permeant Li loss, increased cell resistance, and rapid capacity fading in Si−sulfur batteries.[19] Furthermore, CE and cycling stability of graphite−sulfur batteries could be greatly reduced, when a sulfur cathode with 2 mg cm^{-2} sulfur loading was used.[22] Therefore, it is imperative to develop an effective strategy to minimize polysulfide shuttle effect on those alternative anodes to enable high-performance practical Li-ion sulfur batteries.

Polysulfide shuttle reactions on the non-Li anodes mainly occur in the following steps (as illustrated in Figure 1a). First,

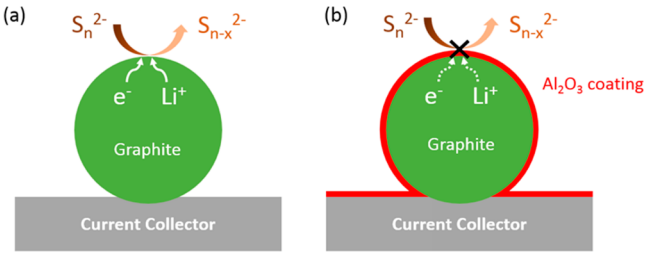

Figure 1. Schematic diagram of (a) polysulfide reduction reactions on the graphite anode surface. (b) Surface passivation layer on the graphite anode blocks the transport pathway for electrons or Li ions, therefore, suppressing polysulfide reduction reactions.

long-chain polysulfides (Li_2S_8, Li_2S_6) mitigate from the cathode to the anode. Then electrons and Li ions from the anode diffuse to the surface, where long-chain polysulfide undergoes an electrochemical reduction described as follows:[5,23]

$$(n-1)Li_2S_n + 2Li^+ + 2e^- \rightarrow nLi_2S_{n-1} \quad (1)$$

The produced short-chain polysulfide will either diffuse back to the cathode causing shuttle reactions or deposit on the surface of anode leading to increased charge transfer resistance. A prerequisite for the polysulfide shuttle reaction is the accessible electron and Li-ion transport from the anode to polysulfide (Figure 1a). Therefore, it is hypothesized that blocking electron or Li-ion transfer from anode to polysulfide would disable chemical/electrochemical reduction of polysulfide, therefore mitigating polysulfide shuttle and improving the battery efficiency.

Herein, we propose to use an ultrathin coating layer (Al_2O_3) to passivate the surface of the non-Li anodes, with the aim of slowing down the electron or Li-ion transfer from anode bulk to anode surface and alleviating polysulfide shuttle (as illustrated in Figure 1b). Graphite is selected as the example in this case for two main reasons. First, graphite has much less volume change during lithiation/delithiation process than other non-Li anodes, such as Si or Sn.[18,19] Large volume change in Si could generate fresh surface that would readily react with polysulfide, thus complicating situation for validating the proposed passivation concept. Second, graphite is commercially available at large scale and lower cost compared to other non-Li anode, and could be potentially adopted in Li-ion sulfur batteries for practical application. Atomic layer deposition (ALD) technique was employed to deposit the Al_2O_3 surface passivation layer on the graphite anode, because ALD possesses an exclusive capability of coating uniform and conformal thin films with thickness controlled at an atomic level[24,25] and have been successfully used to improve the performance of graphite in Li-ion batteries.[26,27]

ALD has been widely adopted to coat surface protection layers on the anode and cathode of Li-ion batteries, thereby reducing unwanted side reactions and improving their energy density, lifetime, and efficiency.[24−34] In this work, Al_2O_3 passivation layers with different thicknesses (1, 2, and 4 nm) were deposited directly on the graphite anode by ALD. Both pristine and Al_2O_3-coated graphite were paired with sulfur cathodes to investigate the effects of anode surface passivation on the CE and capacity retention of graphite-sulfur batteries. Underlying mechanism of anode surface passivation on suppressing polysulfide shuttle reactions was elucidated.

2. EXPERIMENTAL SECTION

2.1. Electrode Preparation. The graphite electrode was prepared from graphite, super-P, and polyvinylidene fluoride (PVDF) (weight ratio = 91:1:8) at the pouch cell line in Advanced Battery Facility at Pacific Northwest National Laboratory. The graphite loading was ∼5.6 mg cm^{-2}. Then Al_2O_3 passivation layers was deposited on the graphite electrode at 100 °C in a Savannah 100 ALD system using trimethylaluminum (TMA) and water as precursors. Al_2O_3 passivation layers with 1 nm, 2 and 4 nm thicknesses were deposited by using 10, 20, and 40 ALD cycles, respectively (with Al_2O_3 growth rate of ∼0.1 nm/cycle). The sulfur cathode was prepared from Integrated Ketjen Black/sulfur (IKB/S, 80 wt % sulfur loading), carbon nanofibers (CNF), and CMC/SBR (weight ratio = 80:10:6/4).[13] To prepare the sulfur cathode, IKB/S composite was first mixed with CNF and CMC in a Thinky mixer at a speed of 1900 r min^{-1} (15 min, mix mode) and subsequently 2000 r min^{-1} (15 min, deform mode) using water as a solvent and n-butanol as an additive. Then SBR was added into the above slurry, which was mixed again following the same procedure. The obtained slurry was coated onto an aluminum foil and the sulfur electrode was dried under vacuum at 60 °C overnight. Mass loading of sulfur on the sulfur cathode was ∼1.6 mg cm^{-2}. Both the graphite and sulfur electrodes were cut into round electrodes with a diameter of 9/16 in. for battery assembly.

2.2. Electrochemical Measurement. The electrolyte used was 5 M lithium bis(trifluoromethanesulfonyl) imide (LiTFSI) dissolved in a 1,3-dioxolane (DOL) solvent.[17] The graphite anode was prelithiated by pressing it directly on a Li metal foil with several drops of 5 M LiTFSI/DOL electrolyte added in between. The color of graphite anode changed from black to yellow after full prelithiation. Then, the prelithiated graphite was coupled with the sulfur electrode in CR2032 coin-type cells, with a Celgard 2500 separator and 5 M LiTFSI/DOL electrolyte (100 μL). The cycling stability was measured at 0.1 C (1 C = 1000 mAh g^{-1}) in a voltage range of 1.7−2.8 V on a LAND battery tester at 30 °C. Electrochemical impedance testing was performed in a frequency range of 0.001−10^6 Hz on a Solartron SI 1260. The specific capacity of the IKB/S cathode was calculated based on the mass of sulfur on the cathode.

2.3. Physical Characterization. Morphology and structure of graphite electrodes were characterized using scanning electron microscopy (SEM, Environmental Field Emission, Inc., Quanta) equipped with Energy Dispersive Spectroscopy (EDS), high resolution transmission electron microscopy (Titan 80−300), and X-ray diffraction (XRD). X-ray photoelectron spectroscopy (XPS) analysis was carried out using an America thermos ESCALAB250 instrument.

DOI: 10.1021/acsami.8b02381
ACS Appl. Mater. Interfaces 2018, 10, 21965−21972

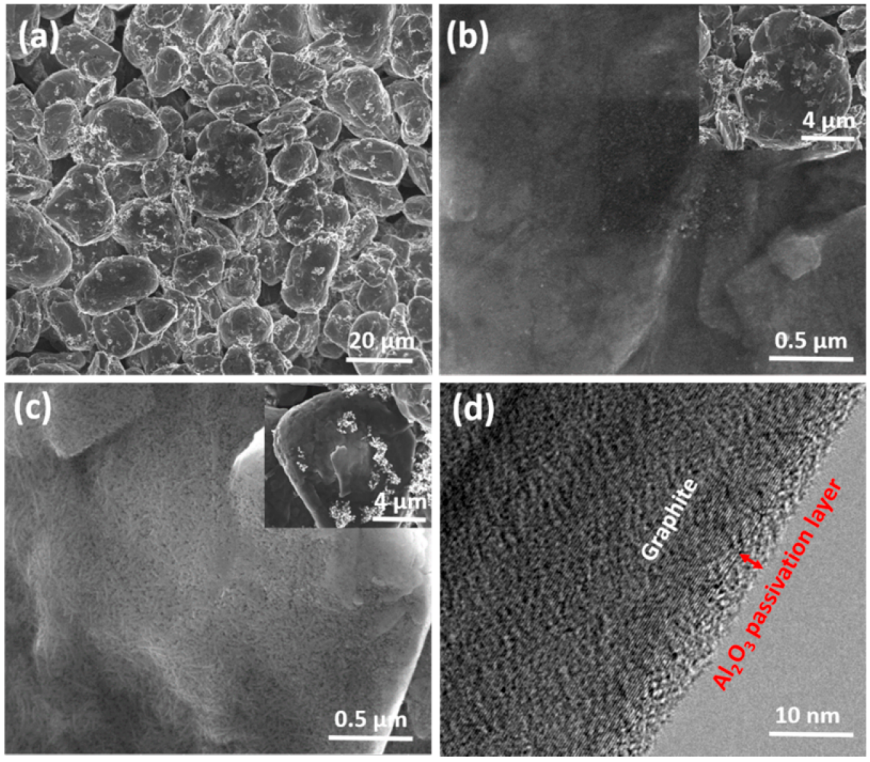

Figure 2. SEM images of (a, b) pristine graphite and (c) 4 nm Al_2O_3/graphite. (d) HRTEM image of 2 nm Al_2O_3/graphite.

3. RESULTS AND DISCUSSIONS

The morphologies of graphite electrodes before and after Al_2O_3 coatings were presented in Figure 2a–2c. The pristine graphite particles are about 20–50 μm in size and have smooth surface (Figure 2a and 2b). The surface of graphite particles becomes uniform textile structure after coating with 40-ALD cycle Al_2O_3, and turns out to be brighter than the pristine graphite under SEM observation (Figure 2b, 2c), due to the charging effect arising from the nonconductive Al_2O_3 layer. High-resolution transmission electron microscopy (HRTEM) analysis reveals a disordered structure of the Al_2O_3 passivation layer (Figure 2d). The thickness of Al_2O_3 layer coated with 20 ALD cycles is measured to be ~2 nm, which corresponds well to the growth rate of Al_2O_3.[25] Furthermore, EDS spectrum confirms the existence of Al element in 20-ALD cycle Al_2O_3 coated on graphite (Figure S1). The above results indicate the successful deposition of Al_2O_3 passivation layers on the graphite electrode.

Graphite anodes with/without Al_2O_3 passivation layers are paired with IKB/S sulfur cathodes (~1.6 mg cm^{-2}) to investigate the influence of Al_2O_3 passivation layers on polysulfide shuttle reactions. Prior to the battery assembly, the graphite anodes are prelithiated by directly contacting with Li metal foils, with a few drops of 5 M LiTFSI/DOL electrolyte added in between. After prelithiation, the color of graphite electrodes changes from black to yellow, and the (002) XRD peak of graphite shifts from 26.4° to 24.2° (Figure S2), both indicating full lithiation of the graphite electrode. 5 M LiTFSI/DOL, instead of 1 M LiTFSI/DOL:DME electrolyte, is used in this work, because the concentrated one was found to help form a stable SEI on the graphite surface and alleviate Li-ion solvent cointercalation into the graphite layers in our previous studies.[22,35] In the LiTFSI/DOL:DME electrolyte, Li-ion solvent would intercalate into the graphite lattices, resulting in exfoliated and amorphous structure and rapid performance degradation due to the lack of SEI layers.[22] Figure 3a and 3b compare the cycling stability and CE of the sulfur cathodes with pristine graphite and graphite coated with 1, 2, and 4 nm Al_2O_3 layers (hereafter denoted as 1, 2, and 4 nm Al_2O_3/graphite, respectively). As seen in Figure 3a, the sulfur cathode with pristine graphite delivers a specific discharge capacity of 900 mAh g^{-1} in the first cycle, and the capacity gradually decreases to 440 mAh g^{-1} after 100 cycles. The quick capacity fading is accompanied by low CE. The first cycle CE is only 84%, and the average CE is about 94% from second to 100th cycle, for the sulfur cathode paired with pristine graphite (Figure 3b). Of note, no $LiNO_3$ additive was used in the electrolyte. For 1 nm Al_2O_3/graphite, the sulfur cathode exhibits slightly higher capacities and much enhanced CE (90% in the first cycle and ~96% afterward), compared to the baseline. The optimal performance of the sulfur cathode is achieved when 2 nm Al_2O_3/graphite is employed. In this case, the sulfur cathode maintains a specific discharge capacity of 550 mAh g^{-1} at the 100th cycle (Figure 3a), and an average CE of 96% from the very first cycle to 100th cycle (Figure 3b). When a thicker Al_2O_3 passivation layer (4 nm) is coated on the graphite anode, the CE of sulfur cathode is kept as similar as in the case of 2 nm Al_2O_3/graphite, but the discharge capacity drops dramatically. The reason for the reduced capacity can be attributed to the thick insulating Al_2O_3 layer, which greatly impedes the lithium ion diffusion and/or electron transfer across the SEI layer. Figure 3c and 3d illustrates the charge/discharge curves of sulfur cathodes with pristine graphite and 2 nm Al_2O_3/graphite anode, respectively. In the first cycle, the sulfur cathode with pristine graphite exhibits a flat second discharge plateau at 1.9 V, corresponding to the transition from long-chain polysulfide to short-chain ones.[6] In comparison, the sulfur cathode with 2 nm Al_2O_3/graphite shows a sloped second discharge plateau until the end of discharge, indicating the poor kinetics of Li–S redox reactions. This abnormal discharge

DOI: 10.1021/acsami.8b02381
ACS Appl. Mater. Interfaces 2018, 10, 21965–21972

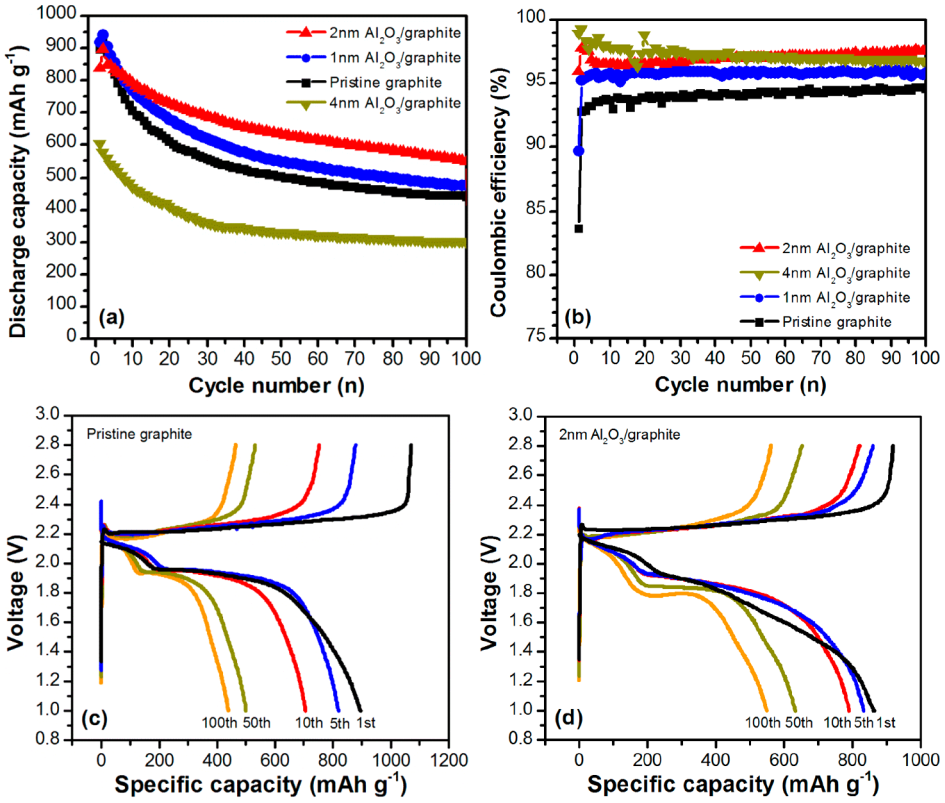

Figure 3. (a) Cycling stability and (b) CE of graphite-sulfur batteries using pristine graphite and 1, 2, and 4 nm Al_2O_3/graphite as the anode; charge−discharge profiles at the 1st, 5th, 50th, and 100th cycles of graphite−sulfur batteries using (c) pristine graphite and (d) 2 nm Al_2O_3/graphite.

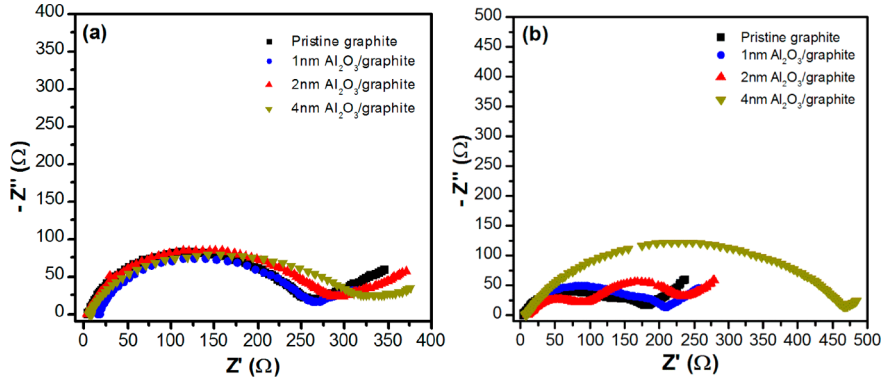

Figure 4. Nyquist plots of graphite−sulfur batteries with/without Al_2O_3 passivation on graphite anode (a) before cycling and (b) after 100 cycles at the charge state.

behavior is only observed in the first cycle, and suggests an "activation" process for the Al_2O_3 passivation layer.[32,33] Another obvious difference in Figure 3c and 3d is the discharge capacity contributed from the first plateau (sulfur to long-chain polysulfide). For the pristine graphite cell, the first-plateau discharge capacity of sulfur cathode gradually reduces from 215 mAh g^{-1} in the second cycle to 122 mAh g^{-1} in the 100th cycle. While for 2 nm Al_2O_3/graphite cell, the first-plateau discharge capacity is maintained at 200 mAh g^{-1} from the second to 100th cycle. Results in Figure 3 indicate that a thin Al_2O_3 passivation layer on the graphite anode could effectively improve the CE and discharge capacity of the sulfur cathode in graphite-sulfur batteries.

To identify the reasons behind the improved performance by Al_2O_3 anode passivation, electrochemical impedance spectroscopy (EIS) analysis is performed on graphite−sulfur batteries before/after cycling, and the results are compared in Figure 4. Before cycling, all graphite−sulfur batteries exhibit similar EIS responses with one semicircle in high and medium frequency ranges (Figure 4a). The semicircle diameter gradually enlarges with the increase of Al_2O_3 coating thickness, suggesting the elevated charge transfer resistance on the graphite anode because of the nonconductive nature of Al_2O_3 layer for Li ions at the deposited state.[26,27,31] Similar trend is also observed in the overall resistance of graphite−sulfur batteries at the charge condition after 100 cycles (Figure 4b). Notably, two semicircles can be clearly identified in the EIS plots for pristine graphite, 1 and 2 nm Al_2O_3/graphite cells. With increasing thickness of Al_2O_3 layers, there is a gradual increase in the semicircle at the medium frequency which might be attributed to the charge transfer resistance from the graphite anode due to the insulating Al_2O_3 coating. A significant increase in the overall resistance is

DOI: 10.1021/acsami.8b02381
ACS Appl. Mater. Interfaces 2018, 10, 21965−21972

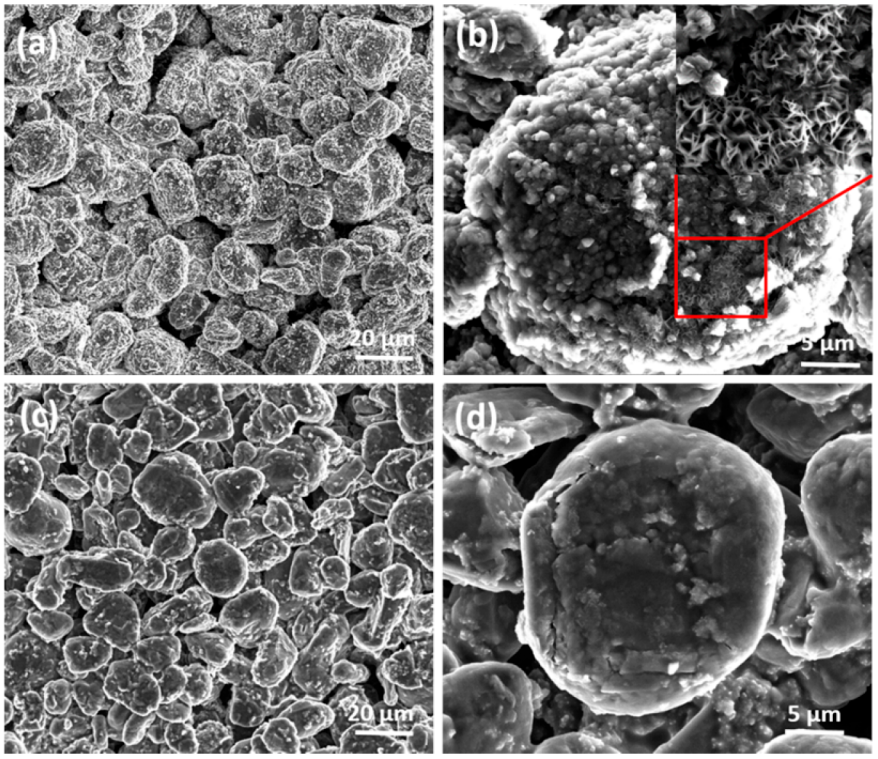

Figure 5. SEM images of (a, b) pristine graphite and (c, d) 2 nm Al_2O_3/graphite anodes after cycling.

found in graphite−sulfur batteries with 4 nm Al_2O_3/graphite (Figure 4b). The EIS results explain the CE and cycling performance of graphite−sulfur batteries shown in Figure 3. A thin Al_2O_3 layer (2 nm) on the graphite particles can reduce electron or Li-ion transfer to the graphite surface and slightly increase the electrode charge transfer resistance, which in turn suppresses polysulfide shuttle reactions and improves the efficiency of graphite−sulfur batteries. While a thick Al_2O_3 layer (4 nm) seriously impedes the diffusion of electrons and lithium ions across the SEI layer, resulting in much higher charge transfer resistance and reduced overall battery performance. The function of Al_2O_3 passivation layers is further confirmed by testing this group of graphite electrodes with Li metal anode using 5 M LiTFSI/DOL electrolyte. The results showed that the capacity of graphite anode is significantly reduced with a 4 nm Al_2O_3 passivation layer, but remains almost the same for 1 and 2 nm Al_2O_3 coatings (Figure S3). The results in Figures 3 and 4 suggest that the thickness of Al_2O_3 passivation layer is critical for achieving the optimal performance of graphite−sulfur batteries. As Al_2O_3 passivation layer increases the charge transfer resistance at graphite anode, we performed electrochemical analysis to have better understanding on the rate capability of different graphite-sulfur batteries. Figure S4 compares the discharge profiles of pristine graphite, 2 nm, and 4 nm Al_2O_3/graphite coupled with sulfur electrodes at current densities of 0.1, 0.5, and 1 C. 2 nm Al_2O_3/graphite shows similar discharge capacity but slightly lower discharge plateau compared with pristine graphite at various current densities, proving that the rate capability of graphite−sulfur batteries is not affected by 2 nm Al_2O_3 layer. However, we observe obvious capacity decrease and polarization in 4 nm Al_2O_3/graphite, suggesting that 4 nm Al_2O_3 layer significantly hinders electrochemical reactions as also reflected in high charge transfer resistance (Figure 4b). On the basis of the above electrochemical results, we believe that Al_2O_3 passivation layer on one hand could suppress polysulfide reactions by blocking electron transfer (pro) and, on the other hand, could also impede Li ion diffusion (con) if the Al_2O_3 layer is too thick (more than 2 nm). For example, in 4 nm Al_2O_3/graphite case, the CE is the highest one in the first 30 cycles (Figure 3b), because thick Al_2O_3 layer can greatly reduce electron transfer, resulting in least shuttle reaction and highest efficiency. At the same time, thick Al_2O_3 layer slows down Li ion diffusion from electrolyte to graphite, leading to low utilization of graphite material and thus low reversible capacity. In pristine graphite case, quick electron transfer at graphite surface allows most shuttle reaction and lowest efficiency (Figure 3b). Meanwhile, fast Li ion diffusion through SEI layer results in highest usage of graphite material and high capacity at beginning, which rapidly decreases due to the deposition of solid Li sulfide on graphite surface. The 2 nm Al_2O_3/graphite reaches a good balance between blocking electron transfer (low shuttle reaction and high efficiency) and maintaining good Li ion diffusion (high capacity).

The morphology and chemical composition of SEI layers on pristine graphite and 2 nm Al_2O_3/graphite anodes after cycling are characterized by SEM and XPS. Compared to the graphite before cycling (Figure 2a and 2b), the one after cycling is totally covered with a thick and rough SEI layer, as seen in Figure 5a and 5b. Flake-like structure can be easily found on the graphite particle surface (insert of Figure 5b), and is identified as solid Li polysulfide or sulfide by EDS analysis (Figure S5). In contrast, 2 nm Al_2O_3/graphite anode after cycling possesses a smooth surface, with no obvious flake-like structure found (Figure 5c and 5d). The observation in Figure 5 suggests that the Al_2O_3 passivation layer reduce the SEI formation and insoluble polysulfide deposition on graphite anode as a result of blocked electron and/or Li ion transfer between graphite and polysulfides. XPS full survey confirms the presence of S, F, C, Li, O,

DOI: 10.1021/acsami.8b02381
ACS Appl. Mater. Interfaces 2018, 10, 21965−21972

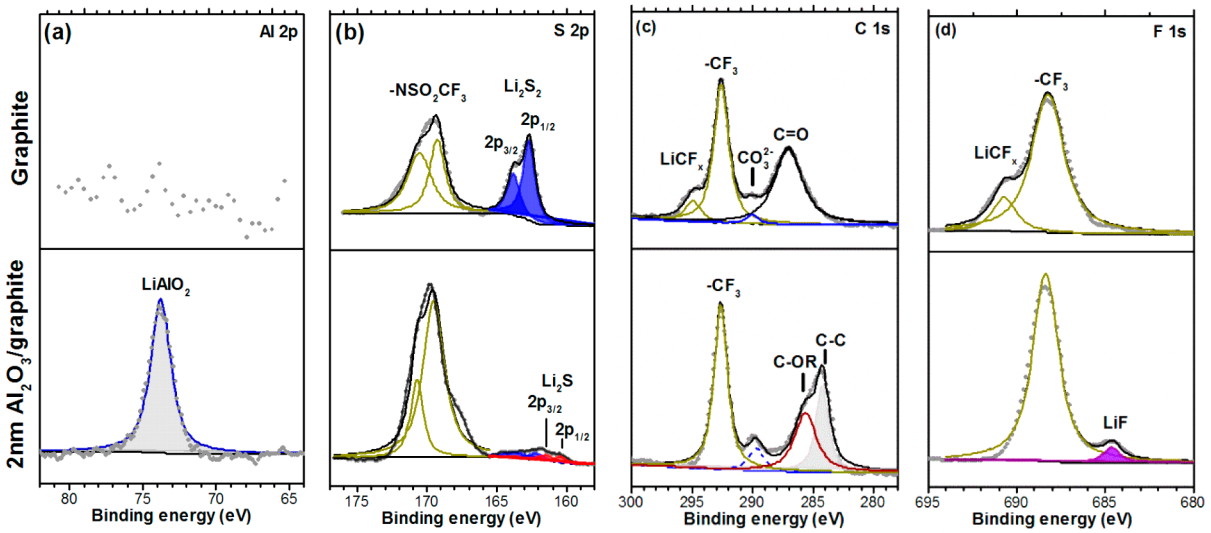

Figure 6. XPS deconvolution of (a) Al_{2p}, (b) S_{2p}, (c) C_{1s}, and (d) F_{1s} spectra for pristine graphite and 2 nm Al_2O_3/graphite after cycling.

and N in SEI layers on graphite and 2 nm Al_2O_3/graphite, with Al element showing up only in the latter (Figures 6 and S6). As seen in Figure 6a, The Al_{2p} spectrum is deconvoluted into one peak at a binding energy of 73.7 eV, which can be assigned to $LiAlO_2$ ion-conductor and is clearly distinguished from that for Al_2O_3 (75.3 eV).[32−34] The Al_{2p} spectrum analysis reveals that the as-deposited Al_2O_3 layer on graphite changes to $LiAlO_2$ during cycling. This change is speculated to happen mainly during the first cycle and correspond to the "activation" process (sloped discharge plateau) in the first discharge cycle of the sulfur cathode with 2 nm Al_2O_3/graphite (Figure 3d). Figure 6b shows that the deconvolution of S_{2p} spectrum of graphite anode consists of two pairs of $2p_{3/2}$ and $2p_{1/2}$ peaks at 163.8 eV/162.6 eV and 170.6 eV/169.3 eV, which correspond well to Li_2S_2 and $-NSO_2CF_3$ species (LiTFSI salt), respectively.[36−39] For 2 nm Al_2O_3/graphite, besides the peaks attributable to Li_2S_2 and $-NSO_2CF_3$, another doublet shows up at binding energies of 161.4 and 160.4 eV and originates from Li_2S.[36,37] A distinct difference in the S 2p peak is the relative higher intensity ratio of insoluble polysulfide to LiTFSI in graphite (0.57) than that in 2 nm Al_2O_3/graphite (0.08). The atomic percentage of sulfur from polysulfide in the SEI layer is calculated to be 2.7 at% and 0.6 at% for graphite and 2 nm Al_2O_3/graphite, respectively (Table S1). This difference further proves the much less polysulfide deposition on the 2 nm Al_2O_3/graphite than on the pristine graphite, in agreement with SEM observation in Figure 5. The occurrence of more LiTFSI salt component on 2 nm Al_2O_3/graphite suggests a more stable SEI on its surface that reduce the interaction of LiTFSI salt with graphite. For the C_{1s} spectra in Figure 6c, one apparent difference between the two samples is that C−C peak located at 284.2 eV appears in 2 nm Al_2O_3/graphite, but in graphite.[40] The C−C peak originates from graphitic carbon of 2 nm Al_2O_3/graphite, suggesting the thin SEI layer on the electrode. For 2 nm Al_2O_3/graphite, three additional major peaks are fitted at 292.6, 289.7, and 285.6 eV, which are ascribed to $-CF_3$ (LiTFSI salt), CO_3^{2-} (lithium carbonate), and C-OR (DOL solvent residual or decomposition products), respectively.[40,41] While for pristine graphite, the strong peak at 287.0 eV is assigned to C═O, which is from DOL decomposition products, and a weak peak at 294.9 eV is ascribed to $LiCF_x$ resulting from LiTFSI salt decomposition.[40,41] $LiCF_x$ is confirmed in the F_{1s} spectrum of graphite (290.6 eV), as shown in Figure 6d. A small F_{1s} peak at 684.6 eV is only found in 2 nm Al_2O_3/graphite, and can be assigned to LiF, an insulting byproduct from LiTFSI decomposition.[37] The LiF component in SEI layer should contribute to the increased charge transfer resistance in 2 nm Al_2O_3/graphite (Figure 4b). The above results indicate that a thin Al_2O_3 passivation layer on the graphite anode has profound impact on the CE and capacity of graphite−sulfur batteries, and the reasons could be attributed to the following two points. First, the Al_2O_3 passivation layer reduces the polysulfide shuttle reactions and polysulfide deposition on graphite anode by slowing down electron or Li ion transfer from graphite to polysulfide, thereby improving the efficiency of graphite-sulfur batteries. Second, the Al_2O_3 passivation layer also greatly suppresses the decomposition of DOL electrolyte and LiTFSI salt, resulting in a much thin, stable, and low-impedance SEI layer that can prevents the further decomposition of electrolyte and salt on graphite anode. This study demonstrates that anode surface passivation is a promising approach to address polysulfide shuttle problem and suppress interfacial side reactions in Li-ion sulfur batteries, thus improving their overall performance. The main concept of the surface passivation is to alleviate side reactions between the anode with polysulfide, electrolyte, and salt. Therefore, this approach can be generally applied to other types of non-Li anodes and electrolyte systems for Li-ion sulfur batteries. In particular, surface passivation becomes even critical for anode with large volume change during lithiation/delithiation process, such as Si or Sn.[18,19] The volume change could expose fresh surface in the anode and lead to continuous parasitic reactions at the electrode−electrolyte interfaces. ALD surface passivation is promising for these anodes, because it could buffer the volume change and stabilize the electrode−electrolyte interfaces in sulfur batteries.

4. CONCLUSIONS

An anode surface passivation approach was used to address polysulfide shuttle problem in graphite−sulfur batteries. Al_2O_3 surface passivation layers were directly deposited on the graphite anode by atomic layer deposition method. The Coulombic efficiency and capacity of sulfur cathode were greatly improved by using graphite anode with a 2 nm Al_2O_3 passivation layer. Postcycling analysis revealed that the Al_2O_3 passivation layer

DOI: 10.1021/acsami.8b02381
ACS Appl. Mater. Interfaces 2018, 10, 21965−21972

slightly increased the charge transfer resistance by slowing down electron and/or Li ion transfer, reduced the polysulfide shuttle reactions, and decreased the polysulfide deposition on the graphite anode. Moreover, in comparison to a thick and rough SEI on pristine graphite, a thin and stable SEI layer formed on the graphite anode with a Al_2O_3 passivation layer due to the reduced decompositions of electrolyte/salt and suppressed deposition of solid polysulfide. The thickness of the Al_2O_3 passivation layers was found to be crucial for achieving optimal performance of graphite-sulfur batteries, and could be precisely adjusted by controlling the cycle numbers during atomic layer deposition process.

■ ASSOCIATED CONTENT

Supporting Information

The Supporting Information is available free of charge on the ACS Publications website at DOI: 10.1021/acsami.8b02381.

EDS spectrum of 2 nm Al_2O_3/graphite; XRD patterns of graphite before and after prelithiation; cycling stability and Coulombic efficiency of graphite|Li half cells using pristine graphite and 1, 2, and 4 nm Al_2O_3/graphite as the electrode; XPS survey of pristine graphite and 2 nm Al_2O_3/graphite after 100 cycles; atomic concentrations of SEI layers on pristine graphite and 2 nm Al_2O_3/graphite after 100 cycles as measured by XPS; and comparison of Li-ion sulfur batteries with different prelithiated non-Li metal anode (PDF)

■ AUTHOR INFORMATION

Corresponding Authors

*E-mail: Dongping·Lu@pnnl.gov.
*E-mail: jun.liu@pnnl.gov.

ORCID

Dongping Lu: 0000-0001-9597-8500
Jianming Zheng: 0000-0002-4928-8194
Xueliang Sun: 0000-0003-2881-8237
Chongmin Wang: 0000-0003-3327-0958
Ji-Guang Zhang: 0000-0001-7343-4609
Jun Liu: 0000-0001-8663-7771

Notes

The authors declare no competing financial interest.

■ ACKNOWLEDGMENTS

This work was supported by the Energy Efficiency and Renewable Energy (EERE) Office of Vehicle Technologies of the U.S. Department of Energy (DOE) under Contract No. DEAC02-05CH11231 and DEAC02-98CH10886 for the Advanced Battery Materials Research (BMR) Program and the Laboratory Directed Research and Development Program at Pacific Northwest National Laboratory (PNNL), a multiprogram national laboratory operated by Battelle for the U.S. Department of Energy. The SEM, XPS, and TEM characterization was conducted in the William R. Wiley Environmental Molecular Sciences Laboratory (EMSL). PNNL is operated by Battelle for the DOE under Contract DE-AC05-76RLO1830. Dr. Jian Liu is grateful for the financial support from Canada NSERC Postdoctoral Fellowship (PDF) Program, PNNL Alternate Sponsored Fellowship (ASF) Program, and University of British Columbia.

■ REFERENCES

(1) Manthiram, A.; Fu, Y.; Chung, S. H.; Zu, C.; Su, Y. S. Rechargeable Lithium-Sulfur Batteries. *Chem. Rev.* **2014**, *114*, 11751−11787.

(2) Seh, Z. W.; Sun, Y.; Zhang, Q.; Cui, Y. Designing High-Energy Lithium-Sulfur Batteries. *Chem. Soc. Rev.* **2016**, *45*, 5605−5634.

(3) Service, R. F. Lithium-Sulfur Batteries Poised For Leap. *Science* **2018**, *359*, 1080−1081.

(4) Yu, X.; Manthiram, A. Electrode−Electrolyte Interfaces In Lithium−Sulfur Batteries With Liquid Or Inorganic Solid Electrolytes. *Acc. Chem. Res.* **2017**, *50*, 2653−2660.

(5) Eroglu, D.; Zavadil, K. R.; Gallagher, K. G. Critical Link Between Materials Chemistry And Cell-Level Design For High Energy Density And Low Cost Lithium-Sulfur Transportation Battery. *J. Electrochem. Soc.* **2015**, *162*, A982−A990.

(6) Zhang, S. S. Liquid Electrolyte Lithium/Sulfur Battery: Fundamental Chemistry, Problems, And Solutions. *J. Power Sources* **2013**, *231*, 153−162.

(7) Kang, H. S.; Park, E.; Hwang, J. Y.; Kim, H.; Aurbach, D.; Rosenman, A.; Sun, Y. K. A Scaled-Up Lithium (Ion)-Sulfur Battery: Newly Faced Problems And Solutions. *Adv. Mater. Technol.* **2016**, *1*, 1600052.

(8) Pope, M. A.; Aksay, I. A. Structural Design Of Cathodes For Li-S Batteries. *Adv. Energy Mater.* **2015**, *5*, 1500124.

(9) Liu, X.; Huang, J. Q.; Zhang, Q.; Mai, L. Nanostructured Metal Oxides And Sulfides For Lithium-Sulfur Batteries. *Adv. Mater.* **2017**, *29*, 1601759.

(10) Cao, R.; Xu, W.; Lv, D.; Xiao, J.; Zhang, J. G. Anodes For Rechargeable Lithium-Sulfur Batteries. *Adv. Energy Mater.* **2015**, *5*, 1402273.

(11) Xu, W.; Wang, J.; Ding, F.; Chen, X.; Nasybulin, E.; Zhang, Y.; Zhang, J. G. Lithium Metal Anodes For Rechargeable Batteries. *Energy Environ. Sci.* **2014**, *7*, 513−537.

(12) Lochala, J.; Liu, D.; Wu, B.; Robinson, C.; Xiao, J. Research Progress Toward The Practical Applications Of Lithium−Sulfur Batteries. *ACS Appl. Mater. Interfaces* **2017**, *9*, 24407−24421.

(13) Lv, D.; Zheng, J.; Li, Q.; Xie, X.; Ferrara, S.; Nie, Z.; Mehdi, L. B.; Browning, N. D.; Zhang, J. G.; Graff, G. L.; Liu, J.; Xiao, J. High Energy Density Lithium-Sulfur Batteries: Challenges Of Thick Sulfur Cathodes. *Adv. Energy Mater.* **2015**, *5*, 1402290.

(14) Lin, Z.; Liu, Z.; Fu, W.; Dudney, N. J.; Liang, C. Phosphorous Pentasulfide As A Novel Additive For High-Performance Lithium-Sulfur Batteries. *Adv. Funct. Mater.* **2013**, *23*, 1064−1069.

(15) Kozen, A. C.; Lin, C. F.; Pearse, A. J.; Schroeder, M. A.; Han, X.; Hu, L.; Lee, S. B.; Rubloff, G. W.; Noked, M. Next-Generation Lithium Metal Anode Engineering Via Atomic Layer Deposition. *ACS Nano* **2015**, *9*, 5884−5892.

(16) Huang, C.; Xiao, J.; Shao, Y.; Zheng, J.; Bennett, W. D.; Lu, D.; Saraf, L. V.; Engelhard, M.; Ji, L.; Zhang, J.; Li, X.; Graff, G. L.; Liu, J. Manipulating Surface Reactions In Lithium-Sulfur Batteries Using Hybrid Anode Structures. *Nat. Commun.* **2014**, *5*, 3015.

(17) Lin, Z.; Liu, Z.; Fu, W.; Dudney, N. J.; Liang, C. Lithium Polysulfidophosphates: A Family Of Lithium-Conducting Sulfur-Rich Compounds For Lithium-Sulfur Batteries. *Angew. Chem., Int. Ed.* **2013**, *52*, 7460−7463.

(18) Yang, Y.; McDowell, M. T.; Jackson, A.; Cha, J. J.; Hong, S. S.; Cui, Y. New Nanostructured Li_2S/Silicon Rechargeable Battery With High Specific Energy. *Nano Lett.* **2010**, *10*, 1486−1491.

(19) Elazari, R.; Salitra, G.; Gershinsky, G.; Garsuch, A.; Panchenko, A.; Aurbach, D. Rechargeable Lithiated Silicon-Sulfur (SLS) Battery Prototypes. *Electrochem. Commun.* **2012**, *14*, 21−24.

(20) Brückner, J.; Thieme, S.; Böttger-Hiller, F.; Bauer, I.; Grossmann, H. T.; Strubel, P.; Althues, H.; Spange, S.; Kaskel, S. Carbon-Based Anodes For Lithium-Sulfur Fuel Cells With High Cycle Stability. *Adv. Funct. Mater.* **2014**, *24*, 1284−1289.

(21) Jeschull, F.; Brandell, D.; Edström, K.; Lacey, M. J. A Stable Graphite Negative Electrode For The Lithium-Sulfur Battery,. *Chem. Commun.* **2015**, *51*, 17100−17103.

(22) Lv, D.; Yan, P.; Shao, Y.; Li, Q.; Ferrara, S.; Pan, H.; Graff, G. L.; Polzin, B.; Wang, C.; Zhang, J.; Liu, J.; Xiao, J. High-Performance Li-Ion Sulfur Batteries Enabled By Intercalation Chemistry. *Chem. Commun.* **2015**, *51*, 13454−13457.

DOI: 10.1021/acsami.8b02381
ACS Appl. Mater. Interfaces 2018, 10, 21965−21972

(23) Wild, M.; O'Neill, L.; Zhang, T.; Purkayastha, R.; Minton, G.; Marinescu, M.; Offer, G. J. Lithium Sulfur Batteries, A Mechanistic Review. *Energy Environ. Sci.* **2015**, *8*, 3477−3494.
(24) George, S. M. Atomic Layer Deposition: An Overview. *Chem. Rev.* **2010**, *110*, 111−131.
(25) Puurunen, R. L. Surface Chemistry Of Atomic Layer Deposition: A Case Study For The Trimethylaluminum/Water Process,. *J. Appl. Phys.* **2005**, *97*, 121301.
(26) Wang, H. Y.; Wang, F. M. Electrochemical Investigation Of An Artificial Solid Electrolyte Interface For Improving The Cycle-Ability Of Lithium Ion Batteries Using An Atomic Layer Deposition On A Graphite Electrode. *J. Power Sources* **2013**, *233*, 1−5.
(27) Lee, M. L.; Su, C. Y.; Lin, Y. H.; Liao, S. C.; Chen, J. M.; Perng, T. P.; Yeh, J. W.; Shih, H. C. Atomic Layer Deposition Of Tio_2 On Negative Electrode For Lithium Ion Batteries. *J. Power Sources* **2013**, *244*, 410−416.
(28) Liu, J.; Sun, X. Elegant Design Of Electrode And Electrode/Electrolyte Interface In Lithium-Ion Batteries By Atomic Layer Deposition. *Nanotechnology* **2015**, *26*, 024001.
(29) Knoops, H. C. M.; Donders, M. E.; van de Sanden, M. C. M.; Notten, P. H. L.; Kessels, W. M. M. Atomic Layer Deposition For Nanostructured Li-Ion Batteries. *J. Vac. Sci. Technol., A* **2012**, *30*, 010801.
(30) Xu, J.; Jia, G.; Mai, W.; Fan, H. J. Energy Storage Performance Enhancement By Surface Engineering Of Electrode Materials. *Adv. Mater. Interfaces* **2016**, *3*, 1600430.
(31) Jung, Y. S.; Cavanagh, A. S.; Riley, L. A.; Kang, S. H.; Dillon, A. C.; Groner, M. D.; George, S. M.; Lee, S. H. Ultrathin Direct Atomic Layer Deposition On Composite Electrodes For Highly Durable And Safe Li-Ion Batteries. *Adv. Mater.* **2010**, *22*, 2172−2176.
(32) Xiao, X.; Lu, P.; Ahn, D. Ultrathin Multifunctional Oxide Coatings For Lithium Ion Batteries. *Adv. Mater.* **2011**, *23*, 3911−3915.
(33) Guan, D.; Jeevarajan, J. A.; Wang, Y. Enhanced Cycleability Of $Limn_2o_4$ Cathodes By Atomic Layer Deposition Of Nanosized-Thin Al_2O_3 Coatings. *Nanoscale* **2011**, *3*, 1465−1469.
(34) Wang, D.; Yang, J.; Liu, J.; Li, X.; Li, R.; Cai, M.; Sham, T. K.; Sun, X. Atomic Layer Deposited Coatings To Significantly Stabilize Anodes For Li Ion Batteries: Effects Of Coating Thickness And The Size Of Anode Particles. *J. Mater. Chem. A* **2014**, *2*, 2306−2312.
(35) Lu, D.; Tao, J.; Yan, P.; Henderson, W. A.; Li, Q.; Shao, Y.; et al. Formation Of Reversible Solid Electrolyte Interface On Graphite Surface From Concentrated Electrolytes. *Nano Lett.* **2017**, *17*, 1602−1609.
(36) Xu, C.; Sun, B.; Gustafsson, T.; Edström, K.; Brandell, D.; Hahlin, M. Interface Layer Formation In Solid Polymer Electrolyte Lithium Batteries: An XPS Study. *J. Mater. Chem. A* **2014**, *2*, 7256−7264.
(37) Jaumann, T.; Balach, J.; Klose, M.; Oswald, S.; Eckert, J.; Giebeler, L. Role Of 1,3-Dioxolane And $Lino_3$ Addition On The Long Term Stability Of Nanostructured Silicon/Carbon Anodes For Rechargeable Lithium Batteries. *J. Electrochem. Soc.* **2016**, *163*, A557−A564.
(38) Zheng, J.; Gu, M.; Chen, H.; Meduri, P.; Engelhard, M. H.; Zhang, J. G.; Liu, J.; Xiao, J. Ionic Liquid-Enhanced Solid State Electrolyte Interface (SEI) For Lithium-Sulfur Batteries. *J. Mater. Chem. A* **2013**, *1*, 8464−8470.
(39) Li, W.; Yao, H.; Yan, K.; Zheng, G.; Liang, Z.; Chiang, Y. M.; Cui, Y. The Synergetic Effect Of Lithium Polysulfide And Lithium Nitrate To Prevent Lithium Dendrite Growth. *Nat. Commun.* **2015**, *6*, 7436.
(40) Aurbach, D.; Pollak, E.; Elazari, R.; Salitra, G.; Kelley, C. S.; Affinito, J. On The Surface Chemical Aspects Of Very High Energy Density, Rechargeable Li-Sulfur Batteries. *J. Electrochem. Soc.* **2009**, *156*, A694−A702.
(41) Busche, M. R.; Drossel, T.; Leichtweiss, T.; Weber, D. A.; Falk, M.; Schneider, M.; Reich, M. L.; Sommer, H.; Adelhelm, P.; Janek, J. Dynamic Formation Of A Solid-Liquid Electrolyte Interphase And Its Consequences For Hybrid-Battery Concepts. *Nat. Chem.* **2016**, *8*, 426−434.

DOI: 10.1021/acsami.8b02381
ACS Appl. Mater. Interfaces 2018, 10, 21965−21972